EUROPEAN ORGANIZATION FOR NUCLEAR RESEARCH

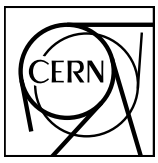

CERN-EP-2022-068
24 March 2022

# Dielectron production at midrapidity at low transverse momentum in peripheral and semi-peripheral Pb–Pb collisions at $\sqrt{s_{\rm NN}} = 5.02$ TeV

ALICE Collaboration



**Abstract**

The first measurement of the $e^+e^-$ pair production at low lepton pair transverse momentum ($p_{\rm T,ee}$) and low invariant mass ($m_{\rm ee}$) in non-central Pb–Pb collisions at $\sqrt{s_{\rm NN}} = 5.02$ TeV at the LHC is presented. The dielectron production is studied with the ALICE detector at midrapidity ($|\eta_{\rm e}| < 0.8$) as a function of invariant mass ($0.4 \leq m_{\rm ee} < 2.7$ GeV/$c^2$) in the 50–70% and 70–90% centrality classes for $p_{\rm T,ee} < 0.1$ GeV/$c$, and as a function of $p_{\rm T,ee}$ in three $m_{\rm ee}$ intervals in the most peripheral Pb–Pb collisions. Below a $p_{\rm T,ee}$ of 0.1 GeV/$c$, a clear excess of $e^+e^-$ pairs is found compared to the expectations from known hadronic sources and predictions of thermal radiation from the medium. The $m_{\rm ee}$ excess spectra are reproduced, within uncertainties, by different predictions of the photon–photon production of dielectrons, where the photons originate from the extremely strong electromagnetic fields generated by the highly Lorentz-contracted Pb nuclei. Lowest-order quantum electrodynamic (QED) calculations, as well as a model that takes into account the impact-parameter dependence of the average transverse momentum of the photons, also provide a good description of the $p_{\rm T,ee}$ spectra. The measured $\sqrt{\langle p_{\rm T,ee}^2 \rangle}$ of the excess $p_{\rm T,ee}$ spectrum in peripheral Pb–Pb collisions is found to be comparable to the values observed previously at RHIC in a similar phase-space region.

## 1 Introduction

Ultra-relativistic heavy-ion collisions produce one of the strongest electromagnetic (EM) fields in the known universe. The magnetic field generated by the highly Lorentz-contracted passing nuclei is predicted to reach up to $10^{15}$ Tesla [1]. Such strong EM fields are predicted to produce various exotic phenomena [2–5]. Heavy-ion collisions have therefore, in the past decades, induced a large amount of experimental and theoretical interest in the search for new aspects of quantum chromodynamics (QCD) and quantum electrodynamics (QED) [6–9].

The measurement of thermal dileptons from the quark–gluon plasma and the hot hadron gas produced in heavy-ion collisions has been long recognized as a clean and powerful probe to study the time evolution of the properties of the medium. Another important dilepton production mechanism, in particular at very low lepton pair transverse momentum ($p_{\mathrm{T,ll}}$), is the photon–photon fusion process ($\gamma\gamma \rightarrow \mathrm{l}^+\mathrm{l}^-$). The EM fields surrounding the relativistic heavy ions with large charge number $Z$ can be treated as a flux of quasi-real photons generated coherently, i.e. the charges of the $Z$ protons in the nucleus act coherently leading to a $Z^2$ dependence of the quasi-real photon flux. These photons can interact via the Breit–Wheeler process [10] to produce dileptons. Such an exclusive photon-mediated process was first measured in ultra-peripheral heavy-ion collisions (UPC) by the STAR collaboration at RHIC [11]. The impact parameter ($b$) between the passing nuclei in UPCs can be selected to be large enough that no nuclear overlap occurs, excluding any hadronic interaction. Only recently, the photon–photon production of dileptons has been observed in hadronic heavy-ion collisions (HHIC) by the STAR [12] and ATLAS [13, 14] collaborations. STAR measures dielectrons ($\mathrm{e}^+\mathrm{e}^-$) at midrapidity and small invariant mass $m_{\mathrm{ee}}$ ($0.4 \leq m_{\mathrm{ee}} \leq 2.6$ GeV/$c^2$) in non-central Au–Au and U–U collisions at a center-of-mass energy per nucleon pair of $\sqrt{s_{\mathrm{NN}}} = 200$ GeV and 193 GeV, respectively, whereas ATLAS reports results on dimuon ($\mu^+\mu^-$) production at large $m_{\mu\mu}$ ( $4 \leq m_{\mu\mu} < 45$ GeV/$c^2$) in central, semi-central and peripheral Pb–Pb collisions at $\sqrt{s_{\mathrm{NN}}} = 5.02$ TeV. The produced dileptons originate from quasi-real photons with momenta predominantly in the beam direction, i.e. the transverse component is of the order of $\omega_\gamma/\gamma_{\mathrm{L}}$, where $\omega_\gamma$ is the photon energy and $\gamma_{\mathrm{L}}$ is the Lorentz factor of the colliding nuclei. Therefore the lepton pairs have a very small $p_{\mathrm{T,ll}}$ and the two leptons are nearly back-to-back. ATLAS quantifies the deviation from back-to-back in terms of the acoplanarity ($\alpha$) defined as $1 - \frac{|\varphi^+ - \varphi^-|}{\pi}$ where $\varphi^+$ and $\varphi^-$ are the azimuthal angles of the two muons. Both experiments show a significant broadening of the $p_{\mathrm{T,ee}}$ (STAR) or $\alpha$ (ATLAS) distributions of the lepton pairs increasing for more central collisions in HHIC compared to UPCs. Whereas STAR attributed it to the possible deflection of the leptons by a magnetic field trapped in an electrically conducting QGP, ATLAS estimated that the observed broadening is qualitatively consistent with potential electromagnetic scatterings of the leptons with the hot and dense medium. Nevertheless, both did not take into account the $b$ dependence of the $p_{\mathrm{T,ee}}$ or $\alpha$ distribution of the lepton pairs.

In the past, two main approaches have been used to calculate the photon–photon interactions: the Equivalent Photon Approximation (EPA) [15–17] and lowest-order QED calculations (LOQED) [18, 19]. In the EPA framework, the cross section of the two-photon process in heavy-ion collisions is obtained as a folding of the equivalent number of quasi-real photons $n_1(\omega_{\gamma,1})$ and $n_2(\omega_{\gamma,2})$ from the field of the nucleus 1 and 2, respectively, and the elementary photoproduction cross section $\sigma_{\gamma\gamma\rightarrow \mathrm{l}^+\mathrm{l}^-}$. The latter is given by the polarization-averaged cross section of the Breit–Wheeler process. Originally, the $k_{\mathrm{T}}$-factorisation method as defined in Refs. [20, 21] was used to calculate the transverse momentum ($k_{\mathrm{T}}$) of the quasi-real photons. In such an approach, the shape of the $k_T$-photon distribution is assumed to be independent of the collision impact parameter. Measurements of photon–photon produced dileptons by ATLAS [22] and ALICE [23] in UPCs are relatively well reproduced by calculations based on the EPA as implemented e.g. in STARlight [24]. Nevertheless, more differential measurements in UPCs show a broadening of the azimuthal back-to-back dilepton correlations or $p_{\mathrm{T,ll}}$ distributions, as well as differences in the invariant mass spectra with increasing number of neutrons at forward rapidity in the events [22, 25, 26]. The latter

enables the selection of collisions occuring at small $b$ that contain exclusive dileptons in conjunction with the excitation and dissociation of the passing nuclei. These results demonstrate significant $b$ dependences in the $\gamma\gamma \to \mathrm{e^+e^-}$ process that are not compatible with the $k_{\mathrm{T}}$-factorisation approach. Such $b$ dependences are, on the other hand, predicted by LOQED calculations [27, 28] which show a $k_{\mathrm{T}}$ hardening of the initial-state photons with a decrease of $b$ as a consequence of the spatial distribution of the EM fields. Attempts to implement $b$ dependences in a generalized EPA approach have been performed in Refs. [27–30]. Such calculations predict strong impact parameter dependences of the dilepton $p_{\mathrm{T,ll}}$ distributions but produce an unphysical increase of the cross section at very low $p_{\mathrm{T,ll}}$ [28], related to neglected interference terms. Recently, an approach using the Wigner formalism suggested in Ref. [31] and performed in Refs. [21, 32, 33], was shown to recover the full $b$ dependence of the lowest-order QED calculations.

After including the $b$ dependence of the photon $k_{\mathrm{T}}$ distribution in the calculations, the existing results of STAR [11, 12, 25], ATLAS [13, 14, 22], and CMS [26] in UPC and HHIC are well described within the uncertainties of the data. As a consequence, room for any medium-induced or final-state effect in HHIC is significantly reduced, whereas photon–photon interactions turn out to be useful for mapping the EM fields generated by the highly Lorentz-contracted nuclei. Further properties of the $\gamma\gamma \to \mathrm{e^+e^-}$ process were measured by STAR. In particular, a $\cos(4\Delta\varphi)$ angular modulation, where $\Delta\varphi$ is the azimuthal angle in the laboratory frame between the momentum of the $\mathrm{e^+e^-}$ pair and one of the electrons, was predicted due to the initial linear photon polarization [31, 34]. This feature was confirmed by STAR measurements in UPCs and peripheral Au–Au collisions with hadronic overlap at $\sqrt{s_{\mathrm{NN}}} = 200$ GeV/$c$ [25] and is closely related to the phenomenon of birefringence [35].

Despite the overall good description of the data by the latest calculations, some points deserve further theoretical and experimental investigation, see Ref. [36] for an overview. Among them, the effect of higher-order corrections in the QED predictions is unclear [37, 38]. Due to the large charge carried by the heavy ion, the parameter of the perturbative expansion in such calculations is large. With ALICE, the $\gamma\gamma \to \mathrm{e^+e^-}$ process can be studied in a similar region of phase space as measured by STAR, but in collisions with a much larger Lorentz-boost factor ($\gamma_{\mathrm{L}}^{\mathrm{LHC}} \approx 2700$, $\gamma_{\mathrm{L}}^{\mathrm{RHIC}} \approx 100$). The maximum electric field reached in heavy-ion collisions is of the order of $Ze\gamma_{\mathrm{L}}/d^2$ [37], where $d$ the distance from the ion's center, and is consequently about 30 times larger at the LHC compared to RHIC. The fields vary and act over a short timescale of approximately $d/\gamma_{\mathrm{L}}c$, i.e. $10^{-25}$ ($10^{-23}$) s at the LHC (RHIC). Therefore, measurements of photon–photon production of dielectrons at the LHC would allow the predicted photon kinematic distributions to be experimentally verified for larger expected magnetic fields than at RHIC and could provide further constraints on the mapping of the EM fields produced in heavy-ion collisions, as well as possible medium effects.

In this article, the first measurement of $\mathrm{e^+e^-}$ pairs at low $p_{\mathrm{T,ee}}$ and $m_{\mathrm{ee}}$ at the LHC is presented in peripheral (70–90%) and semi-peripheral (50–70%) Pb–Pb collisions at $\sqrt{s_{\mathrm{NN}}} = 5.02$ TeV. The dielectron production is measured with ALICE at midrapidity ($|\eta_{\mathrm{e}}| < 0.8$) and $p_{\mathrm{T,ee}} < 0.1$ GeV/$c$ from an invariant mass of 2.7 GeV/$c^2$ down to 0.4 GeV/$c^2$. The latter is determined by the minimum $p_{\mathrm{T}}$ required to identify electrons ($p_{\mathrm{T,e}} > 0.2$ GeV/$c$) in the central barrel. The data are compared with the expected dielectron rate from known hadron decays, called the hadronic cocktail, with predictions for thermal radiation from the medium and with recent predictions for coherent photoproduction of dielectrons as a function of $m_{\mathrm{ee}}$. The $p_{\mathrm{T,ee}}$ and $p_{\mathrm{T,ee}}^2$ distributions are extracted in three different $m_{\mathrm{ee}}$ ranges in peripheral Pb–Pb collisions and the extracted value of $\sqrt{\langle p_{\mathrm{T,ee}}^2 \rangle}$ is compared with predictions and to measurements at lower $\sqrt{s_{\mathrm{NN}}}$.

The article is organized as follows. Section 2 contains a brief description of the ALICE apparatus and the data sample used, whereas Section 3 illustrates the analysis steps. In Section 4, the results on dielectron production yields at low $p_{\mathrm{T,ee}}$ within the ALICE acceptance are presented and compared with theoretical calculations and previous measurements at lower $\sqrt{s_{\mathrm{NN}}}$. Section 5 gives a summary and outlook.

## 2 Detector and data samples

A detailed description of the ALICE apparatus and its performance can be found in Refs. [39, 40]. The main detectors used to track and identify electrons[1] at midrapidity ($|\eta_{\mathrm{e}}| < 0.8$) are the Inner Tracking System (ITS) [41], the Time Projection Chamber (TPC) [42], and the Time-Of-Flight (TOF) detector [43]. The ITS consists of six cylindrical layers of silicon detectors, which provide tracking of the charged particles and, together with the TPC, the reconstruction of the primary collision vertex. The innermost layer is installed at a radius of 3.9 cm from the beam axis and is used to reject electrons from photon conversions in the detector material. The TPC detector allows tracks to be reconstructed and charged particles to be identified (PID) via the measurement of the specific energy loss $\mathrm{d}E/\mathrm{d}x$ while the TOF detector contributes to the PID via the measurement of the flight time of the particles. These detectors are placed inside a uniform magnetic field of 0.5 T parallel to the beam direction, provided by a solenoid magnet.

The data samples used in this analysis were collected by ALICE in 2015 and 2018 during Pb–Pb runs at $\sqrt{s_{\mathrm{NN}}} = 5.02$ TeV. Minimum-bias collisions were triggered by requiring the coincidence of signals in the two scintillator arrays of the V0 detectors [44], covering the pseudorapidity ranges $2.8 \leq \eta < 5.1$ and $-3.7 \leq \eta < -1.7$. The time information from the V0 detectors and the neutron Zero Degree Calorimeters (ZDC) [45], as well as the correlation between the number of hits in the ITS and in the TPC are used offline to reduce the background from beam–gas interactions and pile-up collisions to a negligible level. Only events with a primary vertex reconstructed close to the center of ALICE along the beam direction ($|z| < 10$ cm) are considered in the analysis to assure a uniform detector acceptance. The event sample was divided into centrality classes [46] expressed in percentages of the total hadronic cross section using the amplitudes of the signal in the V0 detector. The number of events in each centrality class considered in this analysis, i.e. 50–70% and 70–90%, is about 34 million after the event selection criteria.

## 3 Data analysis

### 3.1 Electron candidate selection

Electron candidates are selected from charged-particle tracks reconstructed in the ITS and TPC in the kinematic range $|\eta_{\mathrm{e}}| < 0.8$ and $p_{\mathrm{T,e}} > 0.2$ GeV/$c$. The track fits are required to include at least 80 out of a maximum of 159 reconstructed space points in the TPC and a hit in at least 4 of the 6 ITS detector layers. The $\chi^2$ per space point measured in the TPC (ITS) must be less than 2.5 (5). In order to reduce the contribution of secondary tracks arising from weak decays and interactions with the detector material, only tracks with a distance-of-closest approach to the reconstructed primary vertex smaller than 1 cm in the plane transverse to the colliding beams and 0.5 cm in the longitudinal direction are used in the analysis. In addition, a hit in the first ITS layer is required to reject electrons originating from real-photon conversions in the detector material of the subsequent ITS layers. Since the electrons originating from the same photon conversion share the same cluster in the ITS layer where they are produced, they can be further suppressed by requiring that a maximum of one ITS cluster attached to the reconstructed track is shared with any other track candidate and is not placed in the first ITS layer.

The electron identification is based on the complementary information provided by the TPC and TOF. The detector PID signal, $n(\sigma_{\mathrm{i}}^{\mathrm{DET}})$, is expressed in terms of the deviation between the measured and expected value of the specific ionisation energy loss in the TPC or time-of-flight in the TOF for a given particle hypothesis $i$ and momentum, normalised to the respective detector resolution. In the TPC, electrons are selected in the range $|n(\sigma_{\mathrm{e}}^{\mathrm{TPC}})| \leq 3$, whereas kaons, protons and pions are rejected with $|n(\sigma_{\mathrm{K}}^{\mathrm{TPC}})| \geq 3$, $|n(\sigma_{\mathrm{p}}^{\mathrm{TPC}})| \geq 3$ and $n(\sigma_{\pi}^{\mathrm{TPC}}) \geq 3.5$, respectively. Electrons with an energy loss in the TPC in the range where the charged kaon and proton bands cross the one of electrons are recovered using

[1] Note that the term 'electron' is used for both electrons and positrons throughout this paper.

the TOF information: tracks which fulfill only the TPC electron selection and pion rejection but have an associated TOF signal with $|n(\sigma_{\mathrm{e}}^{\mathrm{TOF}})| \leq 3$ are accepted. This PID strategy was used successfully in previous ALICE dielectron analyses in pp and p–Pb collisions [47–49]. Averaged over $p_{\mathrm{T}}$, the hadron contamination in the single-electron candidate sample is less than 5% for an electron efficiency of about 80%. The largest hadron contamination, up to about 18% in the 50–70% centrality class, is observed where kaons ($p_{\mathrm{T}} \approx 0.5$ GeV/$c$), protons ($p_{\mathrm{T}} \approx 1$ GeV/$c$), or charged pions ($p_{\mathrm{T}} > 6$ GeV/$c$) have a similar d$E$/d$x$ as electrons in the TPC. Pairs containing a misidentified hadron are further removed during the subtraction of the combinatorial background, thus that the final hadron contamination in the dielectron signal is negligible.

### 3.2 Signal extraction

Electron pairs originating from the same source cannot be identified unambiguously. Therefore, a statistical approach is used to extract the yield of signal pairs ($S$), in which all electrons and positrons in an event are combined to create an opposite charge-sign spectrum ($OS$). The combinatorial background ($B$) is estimated from same-event pairs with the same charge sign ($SS$). In comparison to a mixed-event approach [50], the same charge-sign approximation of the combinatorial background has the advantage to be self-normalized and to contain all residual correlations arising from charge-symmetric processes, such as from conversions of correlated decay photons originating from the same and from decays of different hadrons inside the same jets or in back-to-back jets. A different acceptance for opposite charge-sign and same charge-sign pairs is observed arising from detector geometrical effects, i.e. non-uniformity of the detector performances in azimuthal angle $\varphi$. The correction factor $R_{\mathrm{acc}}$, needed to account for this effect, is calculated with an event-mixing technique detailed in Ref. [51]. Events with similar global properties are grouped together according to the $z$-position of the reconstructed primary vertex, the centrality of the collision, and the event-plane angle estimated with the V0 detector. The factor $R_{\mathrm{acc}}$ is found to be consistent with unity above $m_{\mathrm{ee}}$ of 1 GeV/$c^2$. The signal is then extracted as $S = OS - R_{\mathrm{acc}} \times SS$.

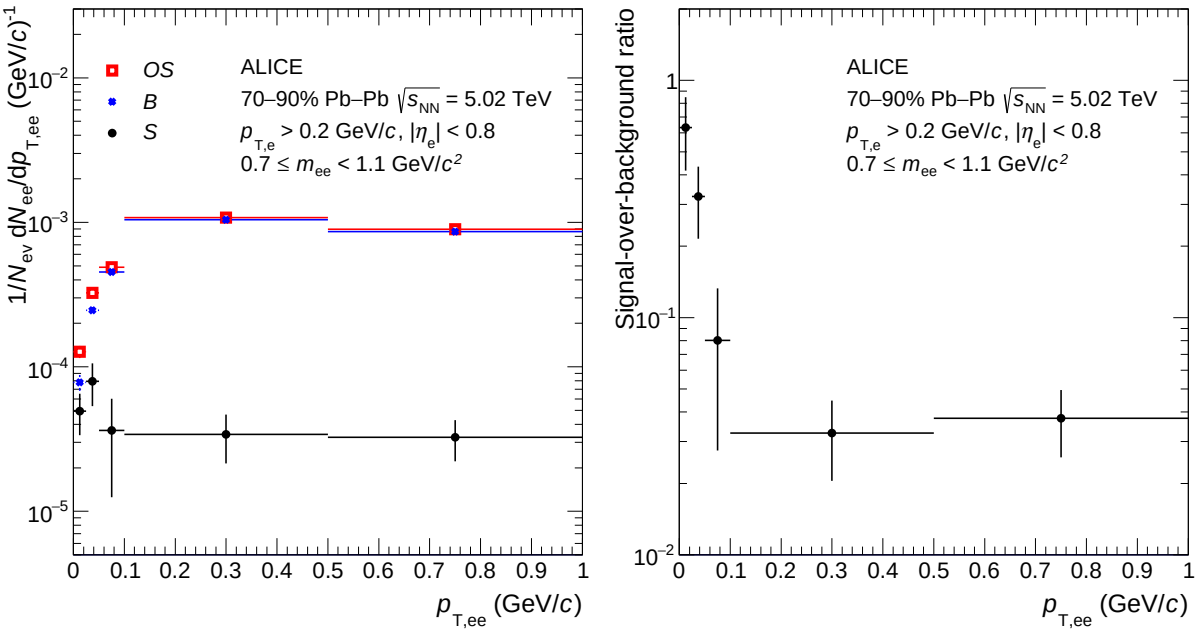


**Figure 1:** Left panel: raw $p_{\mathrm{T,ee}}$-differential yield ($S$) in peripheral (70–90%) Pb–Pb collisions at $\sqrt{s_{\mathrm{NN}}} = 5.02$ TeV for $0.7 \leq m_{\mathrm{ee}} < 1.1$ GeV/$c^2$ overlaid with the opposite charge-sign distribution ($OS$) and the same charge-sign spectrum multiplied by the acceptance correction factor $R_{\mathrm{acc}}$ ($B$). Right panel: signal over background as a function of $p_{\mathrm{T,ee}}$ in peripheral (70–90%) Pb–Pb collisions at $\sqrt{s_{\mathrm{NN}}} = 5.02$ TeV for $0.7 \leq m_{\mathrm{ee}} < 1.1$ GeV/$c^2$.

The opposite charge-sign spectrum, the combinatorial background, and the extracted raw dielectron signal are shown in the left panel of Fig. 1 as a function of the pair transverse momentum $p_{\mathrm{T,ee}}$ for $0.7 \leq m_{\mathrm{ee}} < 1.1$ GeV/$c^2$ in 70–90% peripheral Pb–Pb collisions. The corresponding signal-over-background ratio ($S/B$) is presented in the right panel of Fig. 1. Towards very low $p_{\mathrm{T,ee}}$ ($p_{\mathrm{T,ee}} \leq 0.1$ GeV/$c$), the $S/B$ ratio increases for both centrality classes. However, the $S/B$ ratio is about one order of magnitude lower in the 50–70% centrality class in this $p_{\mathrm{T,ee}}$ region.

### 3.3 Efficiency correction

The raw signal is corrected for the finite dielectron reconstruction efficiency. To this end, different Monte Carlo (MC) simulations are used, where a realistic detector response is modelled using GEANT3 [52]. For very low $p_{\mathrm{T,ee}}$ ($p_{\mathrm{T,ee}} < 0.2$ GeV/$c$), photoproduced $\mathrm{e^+e^-}$ pairs are simulated with the event generator STARlight [24] and embedded into hadronic collisions computed with HIJING [53]. At larger $p_{\mathrm{T,ee}}$, additional samples of dielectron sources injected into HIJING simulated events are utilized. These include light-flavour hadrons ($\pi^0$, $\eta$, $\eta\prime$, $\rho^0$, $\omega$ and $\phi$) and $J/\psi$ mesons, forced to decay into dielectrons with the phenomenological EXODUS generator [50] and PHOTOS [54], respectively, and produced in equal amounts with uniform $p_{\mathrm{T}}$ distributions. In each centrality class (50–70% or 70–90%), these input $p_{\mathrm{T}}$ distributions are corrected with $p_{\mathrm{T}}$-dependent weights defined as the ratio of the hadron $p_{\mathrm{T}}$ spectra in the MC simulations and the expected hadron $p_{\mathrm{T}}$ distributions according to the hadronic cocktail explained in Section 3.5. The weights are passed to the decay electrons to produce a realistic mix of $\mathrm{e^+e^-}$ pairs from the various sources considered. In addition, an enriched sample of heavy-flavour hadron sources with enforced semileptonic decay channels generated with the Perugia 2011 tune of PYTHIA 6.4 [55, 56] is used. The final efficiency as a function of $m_{\mathrm{ee}}$ and $p_{\mathrm{T,ee}}$ is the average of the efficiencies of the different dielectron sources, weighted by their expected contribution, for $p_{\mathrm{T,ee}} \geq 0.2$ GeV/$c$. At lower $p_{\mathrm{T,ee}}$ only the STARlight calculations are taken as input. Other sources show dielectron efficiencies in agreement within statistical uncertainties with the one extracted for $\mathrm{e^+e^-}$ pairs produced via photon–photon interactions.

### 3.4 Systematic uncertainties of measured dielectron spectra

The systematic uncertainties on the measured dielectron spectrum originate from tracking, electron identification and purity, and background subtraction. They are evaluated as described in Ref. [47] and summarised in Table 1 for $p_{\mathrm{T,ee}} < 0.1$ GeV/$c$.

**Table 1:** Summary of the total systematic uncertainties for $p_{\mathrm{T,ee}} < 0.1$ GeV/$c$ in semi-peripheral (50–70%) and peripheral (70–90%) Pb–Pb collisions at $\sqrt{s_{\mathrm{NN}}} = 5.02$ TeV. The values presented as a range correspond to the smallest and largest observed systematic uncertainties.

| Centrality class | Hit in the first ITS layer | TPC–TOF matching | ITS–TPC matching | Shared ITS cluster | Tracking and PID | Anchor point | Total |
|---|---|---|---|---|---|---|---|
| 50–70% | 2% | 0–4% | 5.4–7.4% | 4% | 16% | 0% | 18% |
| 70–90% | 2% | 0–4% | 5.4–7.4% | 4% | 6% | 5% | 10–12% |

The systematic uncertainties related to the requirement of a hit in the innermost ITS layer, the matching of the TPC track and the signal measured in the TOF, and the matching of the track segments reconstructed in the ITS and the TPC are first estimated at the single-track level. To this end, the efficiencies of these selection criteria are compared in data and in MC as a function of $p_{\mathrm{T}}$ for a pure sample of charged pions or electrons (TPC–TOF matching). The latter is obtained by selecting electrons from photon conversions in the detector material using topological requirements. A MC method is then used to calculate the corresponding uncertainties for dielectrons, by generating particles in the full $m_{\mathrm{ee}}$ and $p_{\mathrm{T,ee}}$ phase space and forcing them to decay to $\mathrm{e^+e^-}$ pairs. The uncertainty for each $\mathrm{e^+e^-}$ pair is given by the sum of the uncertainties of the decay electrons, after applying the fiducial selection ($|\eta_{\mathrm{e}}| < 0.8$ and

$p_{\mathrm{T,e}} \geq 0.2$ GeV/$c$). The final systematic uncertainty is obtained after averaging for a given $m_{\mathrm{ee}}$ and $p_{\mathrm{T,ee}}$ over all generated particles. The TPC–TOF matching efficiency is relevant only in the regions where the kaon and proton bands cross the band of electrons in the TPC. The corresponding uncertainty varies between 0 and 4% for the $\mathrm{e}^+\mathrm{e}^-$ pairs and is the largest for the invariant mass bin $1.1 \leq m_{\mathrm{ee}} < 2.7$ GeV/$c^2$ at low $p_{\mathrm{T,ee}}$ ($p_{\mathrm{T,ee}} < 0.1$ GeV/$c$). The ITS–TPC matching efficiency is one of the dominant sources of systematic uncertainties together with the particle identification and leads to uncertainties between 5.4% and 7.4% increasing with $m_{\mathrm{ee}}$. The systematic uncertainty originating from the requirement of a hit in the first ITS layer is of the order of 2%.

The systematic uncertainty from the requirement on the number of ITS shared clusters is estimated by varying the number of allowed shared ITS clusters for the selected electron candidates and repeating the analysis steps. Releasing completely this selection criterion increases significantly the amount of electrons from conversions in the detector material and leads to a smaller S/B by a factor of about 0.6. Therefore the extracted systematic uncertainty contains not only systematic effects from the signal efficiency, but also from the background estimation. It is calculated from the maximum deviations of the efficiency-corrected spectra variations, considered as statistically significant according to the Barlow criterion [57] and found to be of the order of 4%.

In a similar way, the systematic uncertainty arising from the tracking and electron identification and purity is evaluated by varying the remaining electron selection criteria simultaneously, e.g. the requirement on the minimum number of reconstructed space points in the TPC or $|n(\sigma_{\mathrm{e}}^{\mathrm{TPC}})|$. In particular modifying the requirements on the TPC and TOF signals, i.e. $|n(\sigma_{\mathrm{e}}^{\mathrm{TPC}})|$, $|n(\sigma_{\pi}^{\mathrm{TPC}})|$, $|n(\sigma_{\mathrm{K}}^{\mathrm{TPC}})|$, $|n(\sigma_{\mathrm{p}}^{\mathrm{TPC}})|$ and $|n(\sigma_{\mathrm{e}}^{\mathrm{TOF}})|$, enables to probe possible biases due to differences in the detector responses in data and MC and remaining hadron contamination in the electron sample. The systematic uncertainty is computed as the root-mean-square of the variation of the final data points and is found to be of the order of 16% (6%) in semi-peripheral (peripheral) Pb–Pb collisions for $p_{\mathrm{T,ee}} < 0.1$ GeV/$c$. The main source of systematic uncertainty in the 50–70% centrality class comes from the kaon and proton rejection in the TPC and the non-perfect description of the measured particle energy loss in the TPC in the simulations, which depends on the centrality of the collisions.

The systematic uncertainty originating from the correction factor $R_{\mathrm{acc}}$, estimated by varying the event mixing pools used to calculate it, was found to be negligible at low $p_{\mathrm{T,ee}}$.

Finally, systematic uncertainties arise from the centrality class definition. The absolute scale of the centrality is defined by the range of 0–90% centrality in which a Glauber-based multiplicity model is fitted to the V0M distribution [46]. The lower centrality limit of 90% of this range with its corresponding V0M signal is denoted the anchor point (AP). The AP was shifted by $\pm 1$%, leading to a systematic uncertainty of 5% for the 70–90% centrality class and negligible for the 50–70% centrality class.

### 3.5 Expected yield from known hadronic sources

The expected dielectron yield from the decays of known hadrons produced in the hadronic Pb–Pb collisions, called the hadronic cocktail, is calculated with a fast simulation of the ALICE central barrel, including the angular and momentum resolution of the detector and bremsstrahlung effects [58].

The Dalitz and dielectron decays of light neutral mesons are simulated following the approach described in Ref. [59]. The $p_{\mathrm{T}}$-differential production cross sections of $\eta$ and $\omega$ are estimated based on the ratio of their $p_{\mathrm{T}}$ spectra to the one of $\pi^0$ or $\pi^{\pm}$, measured in different collision systems and at different center-of-mass energies, whereas $\eta'$, $\rho$, and $\phi$ are generated assuming $m_{\mathrm{T}}$-scaling over the full $p_{\mathrm{T}}$ range or only at low $p_{\mathrm{T}}$ [60–62]. The $p_{\mathrm{T}}$ spectra of $\pi^{\pm}$, measured down to a $p_{\mathrm{T}}$ of 0.1 GeV/$c$ as a function of the collision centrality in Pb–Pb collisions at $\sqrt{s_{\mathrm{NN}}} = 5.02$ TeV [63], are parametrized and extrapolated to $p_{\mathrm{T}} = 0$ using a two-component function [64, 65]. The difference between $\pi^0$ and $\pi^{\pm}$ due to isospin-violating decays is taken into account using an effective model that describes measured hadron spectra ($\pi^{\pm}$, $\mathrm{K}^{\pm}$,

and p [63]) at low $p_{\mathrm{T}}$ and includes strong and electromagnetic decays [66], as described in Ref. [48]. This leads to $p_{\mathrm{T}}$-dependent scaling factors applied to the $\pi^{\pm}$ parametrizations of about 1.3 for $p_{\mathrm{T}} \to 0$ and consistent with unity within 2% for $p_{\mathrm{T}} > 1$ GeV/$c$. The $p_{\mathrm{T}}$ spectrum of $\eta$ is computed as the average of the spectra obtained using the parametrizations retrieved from the $\eta/\pi^0$ ratio as a function of $p_{\mathrm{T}}$ in pp collisions [48] and from the $\mathrm{K}^{\pm}/\pi^{\pm}$ ratio as a function of $p_{\mathrm{T}}$ measured down to $p_{\mathrm{T}} = 0.3$ GeV/$c$ in Pb–Pb collisions [63]. In all considered centrality classes (50–70% and 70–90%), the ratio of the resulting $p_{\mathrm{T}}$ distribution of $\eta$ to the $\pi^0$ parametrization at very low $p_{\mathrm{T}}$ ($p_{\mathrm{T}} \leq 0.1$ GeV/$c$) was found to be in agreement within uncertainties with the $\eta/\pi^0$ ratio in pp collisions. The latter is constrained at low $p_{\mathrm{T}}$ by the data from CERES/TAPS [67] and has a conservative $p_{\mathrm{T}}$-dependent uncertainty of up to 40%, which is taken into account in the final uncertainty of the hadronic cocktail. At $m_{\mathrm{ee}}$ around 0.782 GeV/$c^2$, the dominant contribution to the hadronic cocktail is given by the $\omega$ meson. A parametrization of the $\omega/\pi^0$ ratio as a function of $p_{\mathrm{T}}$ measured by ALICE in pp collisions at $\sqrt{s} = 7$ TeV [68] is performed and extended to $p_{\mathrm{T}} = 0$ using data from PHENIX in pp collisions at $\sqrt{s} = 200$ GeV [69]. It is used for all centrality classes. Finally, the measured $p_{\mathrm{T}}$ spectra of $\phi$ mesons in semi-central and peripheral Pb–Pb collisions at $\sqrt{s_{\mathrm{NN}}} = 5.02$ TeV [70] are fitted and extrapolated down to low $p_{\mathrm{T}}$ ($p_{\mathrm{T}} \leq 0.4$ GeV/$c$) using $m_{\mathrm{T}}$ scaling to obtain the $\phi$ input parametrizations.

The contribution from correlated semileptonic decays of open charm and beauty hadrons is computed with the next-to-leading order event generator POWHEG [71–74] with PYTHIA 6 [55] to evolve the parton shower. The expected yield is normalized to the cross sections $\mathrm{d}\sigma_{\mathrm{c\bar{c}}}/\mathrm{dy}|_{\mathrm{y=0}}$ and $\mathrm{d}\sigma_{\mathrm{b\bar{b}}}/\mathrm{dy}|_{\mathrm{y=0}}$ extracted with the same MC generator from the $\mathrm{e^+e^-}$ spectra measured in pp collisions at $\sqrt{s} = 5.02$ TeV [47] and scaled with the nuclear overlap function. The uncertainties related to the branching ratio of the semileptonic decays of the open heavy-flavour hadrons and the fragmentation functions of charm and beauty quarks are omitted under the assumption that these do not change from pp to peripheral and semi-peripheral Pb–Pb collisions.

The systematic uncertainties of the hadronic cocktail are computed by adding in quadrature the uncertainties originating from the following sources: the $\pi^{\pm}$ and $\phi$ parametrizations as a function of $p_{\mathrm{T}}$, the $\pi^0/\pi^{\pm}$ correction factor, the $\eta/\pi^0$ and $\omega/\pi^0$ ratios, the $m_{\mathrm{T}}$-scaling parameters used for $\eta'$, $\rho$ and $\phi$, the branching ratios of the different light-flavour hadron decay channels, the heavy-flavour cross sections and the nuclear overlap function. The final systematic uncertainty of the hadronic cocktail at very low $p_{\mathrm{T}}$ ($p_{\mathrm{T,ee}} < 0.1$ GeV/$c$) is between 14% in the intermediate mass range ($1.1 \leq m_{\mathrm{ee}} < 2.7$ GeV/$c^2$) and about 30% in the mass regions dominated by $\eta$ and $\omega$ decays ($m_{\mathrm{ee}} \approx 0.4$ GeV/$c^2$ for $\eta$ and $m_{\mathrm{ee}} \approx 0.782$ GeV/$c^2$ for $\omega$).

## 4 Results

### 4.1 Invariant mass spectra

The efficiency-corrected $\mathrm{e^+e^-}$ invariant mass spectra at low $p_{\mathrm{T,ee}}$ ($p_{\mathrm{T,ee}} < 0.1$ GeV/$c$) are shown in Fig. 2 in peripheral (70–90%) and semi-peripheral (50–70%) Pb–Pb collisions at $\sqrt{s_{\mathrm{NN}}} = 5.02$ TeV within the ALICE acceptance ($|\eta_{\mathrm{e}}| < 0.8$ and $p_{\mathrm{T,e}} > 0.2$ GeV/$c$). In this figure and the following ones, the upper limit at 90% C.L. using the Feldman and Cousins methodology [75] is reported for the results which are found to be statistically consistent with zero within one standard deviation. The data are compared with cocktails of expected $\mathrm{e^+e^-}$ hadronic sources. The corresponding enhancement factors, expressed as ratios of data over hadronic cocktail, are illustrated in the bottom panel of Fig. 2. The total uncertainty of the cocktail is represented by a band. An excess of dielectrons compared to the hadronic expectation is observed in both centrality classes, with a larger significance in peripheral Pb–Pb collisions.

The hadronic cocktail contribution is subtracted from the inclusive $\mathrm{e^+e^-}$ pairs to obtain the invariant mass distributions for excess $\mathrm{e^+e^-}$ pairs with $p_{\mathrm{T,ee}} < 0.1$ GeV/$c$ presented in the left and right panels of Fig. 3 for the 50–70% and 70–90% centrality classes, respectively. The yield of excess $\mathrm{e^+e^-}$ pairs does not

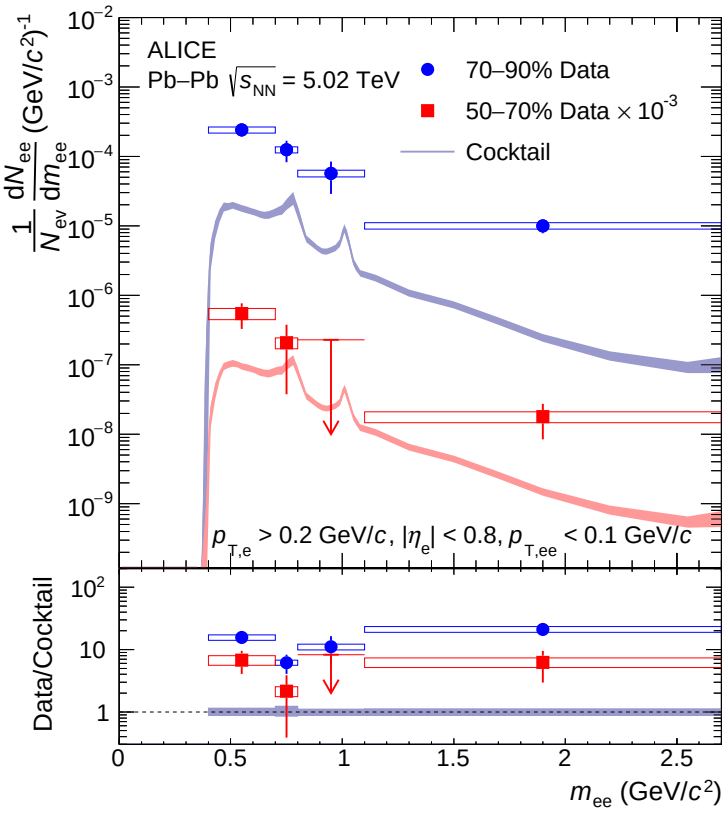


**Figure 2:** Dielectron $m_{\mathrm{ee}}$-differential yields in semi-peripheral (50–70%) and peripheral (70–90%) Pb–Pb collisions at $\sqrt{s_{\mathrm{NN}}}$ = 5.02 TeV, compared with the expected $\mathrm{e^+e^-}$ contributions from known hadronic decays. The error bars and boxes represent the statistical and systematic uncertainties of the data, respectively, whereas the bands show the uncertainties of the hadronic cocktail. Arrows indicate upper limits at 90% confidence level.

show a significant centrality dependence. The expected contributions from thermal dielectrons from the partonic and hadronic phases are also shown in the figure. They are estimated with an expanding thermal fireball model including an in-medium broadened $\rho$ spectral function [76–78]. Predictions from the same model describe well the SPS [79, 80] and RHIC [81, 82] data. At $p_{\mathrm{T,ee}} < 0.1$ GeV/$c$, thermal radiation from the medium is expected to be at least one order of magnitude smaller than the measured $\mathrm{e^+e^-}$ excess in peripheral Pb–Pb collisions and have a different $p_{\mathrm{T,ee}}$ shape and centrality dependence [20]. The excess yield in the $\mathrm{e^+e^-}$ invariant mass spectra are further compared with different calculations for photon–photon production of dielectrons. A QED calculation at leading-order was performed by the authors of Refs. [28, 36]. The lowest-order two-photon interaction is a second-order process with two contributing Feynman diagrams, as shown in Fig. 2 of Ref. [18]. Higher-order contributions are ignored, although the parameter of the perturbative expansion, the coupling $Z\alpha$ with $\alpha$ the fine structure constant, is close to unity, i.e. 0.6, for lead ions. The straight-line approximation for the incoming projectile and target nuclei is applied, as for the other calculations. The predictions from the authors of Ref. [21] employ the Wigner formalism. The quasi-real photon fluxes originating from strong EM fields produced by the highly Lorentz-contracted heavy ions passing each other can be written in terms of Wigner functions in momentum and impact-parameter space. The cross section for the $\gamma\gamma \rightarrow \mathrm{e^+e^-}$ process is then expressed as a convolution over impact parameters and transverse momenta. Realistic charge form factors of the Pb nuclei, i.e Fourier transforms of the charge density, are taken from Ref. [83]. About 50% of the $\mathrm{e^+e^-}$ pairs are produced inside the nuclei for the centrality class 70–90%. The model implemented in the STARlight MC generator uses the equivalent photon approximation approach [24, 84]. The main difference between

STARlight and the two aforementioned calculations is related to the treatment of the $b$ dependence in the computations. STARlight utilizes the $k_{\mathrm{T}}$-factorisation method, where the one-photon distribution is integrated over all transverse distances to obtain the shape of the $k_{\mathrm{T}}$ distribution. For all models, the $m_{\mathrm{ee}}$ and $p_{\mathrm{T,ee}}$ detector resolution, not corrected in the data, are taken into account by folding the momentum and opening angle resolution, including bremsstrahlung effects, in the calculations. All models can reproduce the measured $m_{\mathrm{ee}}$ excess spectra within their uncertainties. The ratios of the measured excess yields to the different calculations, shown in the bottom panels of Fig. 3, are consistent with unity within the statistical and systematic uncertainties of the data in both centrality classes. However, the STARlight predictions appear to be further away from the data than the other calculations. The contributions from decays of vector mesons produced in photo–nuclear collisions are expected to be very small for $\rho$, $\omega$ and $\phi$ [12, 25] and below 5% based on ALICE results for photoproduced $J/\psi$ at forward rapidity in Pb–Pb collisions at $\sqrt{s_{\mathrm{NN}}}$ = 5.02 TeV [85] extrapolated to midrapidity using the IIM model scenario 2 in Ref. [86].

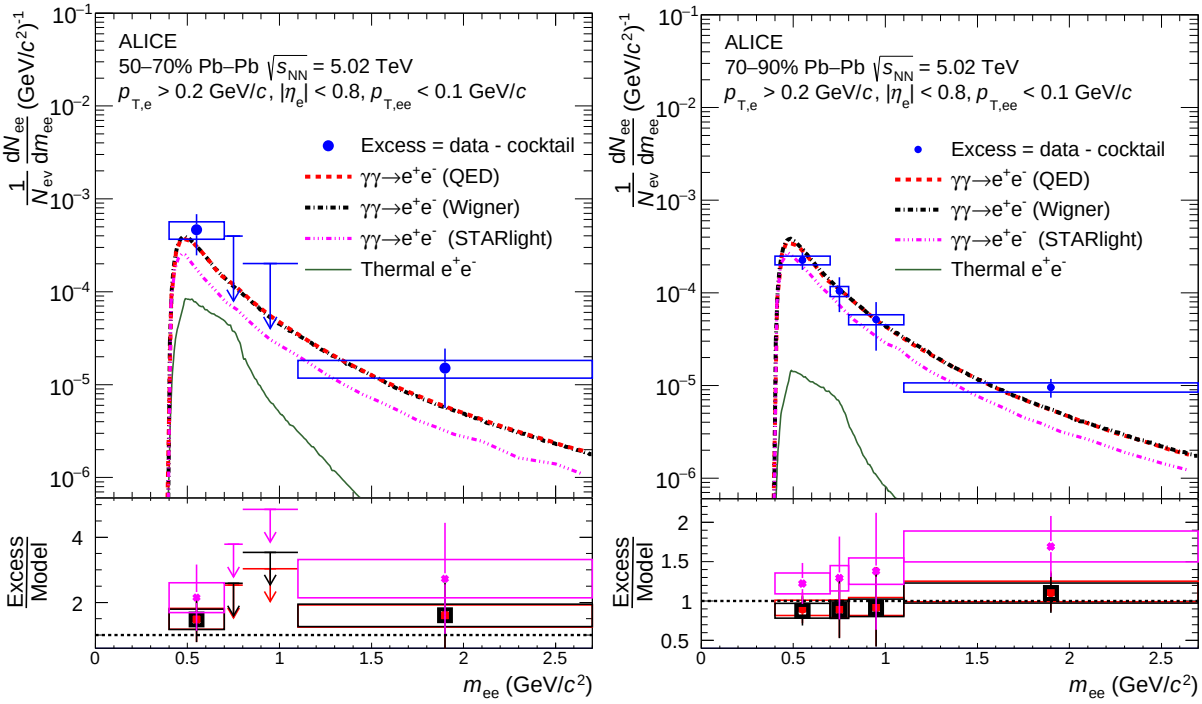


**Figure 3:** Excess dielectron $m_{\mathrm{ee}}$-differential yields after subtraction of the cocktail of known hadronic decay contributions in semi-peripheral (left) and peripheral (right) Pb–Pb collisions at $\sqrt{s_{\mathrm{NN}}}$ = 5.02 TeV, compared with calculations for coherent two-photon production of $\mathrm{e^+e^-}$ pairs folded with the detector resolution [21, 24, 28, 36, 84]. For details see the text. The error bars and boxes represent the statistical and systematic uncertainties of the data, respectively. Arrows indicate upper limits at 90% confidence level.

### 4.2 Transverse momentum spectra

In order to further investigate the dielectrons produced via photon–photon interactions at low $p_{\mathrm{T,ee}}$, the $p_{\mathrm{T,ee}}$ spectra of inclusive $\mathrm{e^+e^-}$ pairs are shown in three different invariant mass ranges in peripheral Pb–Pb collisions at $\sqrt{s_{\mathrm{NN}}}$ = 5.02 TeV in Fig. 4. While the measured yield at $p_{\mathrm{T,ee}} \geq 0.1$ GeV/$c$ can be described by the hadronic cocktail, a clear peak is seen at $p_{\mathrm{T,ee}}$ smaller than 0.1 GeV/$c$ in all $m_{\mathrm{ee}}$ ranges. The latter is fairly well reproduced by the aforementioned photon–photon models including the impact parameter dependence of the photon $k_{\mathrm{T}}$ distribution, i.e. the lowest-order QED calculations [28, 36] and calculations using the Wigner formalism [21]. Both approaches predict very similar $p_{\mathrm{T,ee}}$ distributions. On the contrary, all spectra computed with the STARlight model [24, 84] show a rise towards $p_{\mathrm{T,ee}}$

equal to zero, which is disfavored by the data. By integrating over all transverse distances in the single-photon distribution, the $k_{\mathrm{T}}$-factorization approach employed in STARlight leads to a $p_{\mathrm{T,ee}}$ distribution whose shape is independent of the impact parameter. Such a treatment gives rise to uncertainties on the $k_{\mathrm{T}}$ photon distribution of the order of $\omega_\gamma/\gamma_{\mathrm{L}}$, which is precisely the same order of magnitude as $k_{\mathrm{T}}$ itself [18, 29]. The data confirm that the $b$ dependence of $k_{\mathrm{T}}$, and as a consequence $p_{\mathrm{T,ee}}$, cannot be neglected in non ultra-peripheral heavy-ion collisions. The limited $p_{\mathrm{T}}$ resolution of the detector has a negligible effect compared to the data uncertainties at low $m_{\mathrm{ee}}$ ($0.4 \leq m_{\mathrm{ee}} < 0.7$ GeV/$c^2$) but it affects more significantly the reconstructed $p_{\mathrm{T,ee}}$ distributions at large $m_{\mathrm{ee}}$ ($1.1 \leq m_{\mathrm{ee}} < 2.7$ GeV/$c^2$) reducing the maximum of the spectra predicted with the Wigner formalism and lowest-order QED calculations by about 35%. At large $m_{\mathrm{ee}}$, where electrons have larger $p_{\mathrm{T}}$, the detector resolution on $p_{\mathrm{T}}$ worsens.

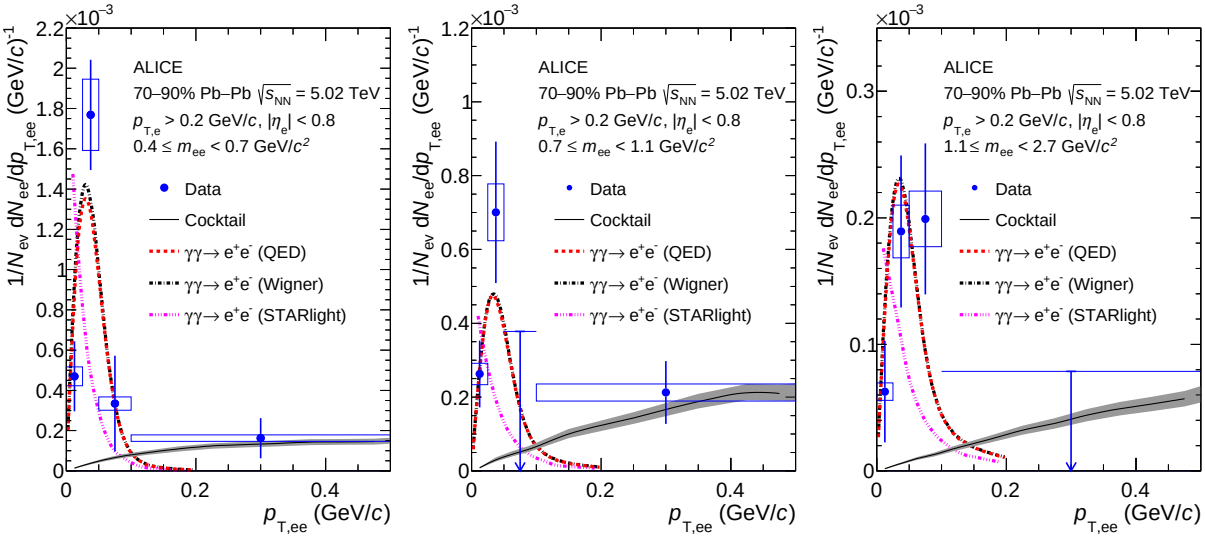


**Figure 4:** Dielectron $p_{\mathrm{T,ee}}$-differential yields in peripheral (70–90%) Pb–Pb collisions at $\sqrt{s_{\mathrm{NN}}} = 5.02$ TeV for three different $m_{\mathrm{ee}}$ ranges, i.e. $0.4 \leq m_{\mathrm{ee}} < 0.7$ GeV/$c^2$ (left), $0.7 \leq m_{\mathrm{ee}} < 1.1$ GeV/$c^2$ (middle), and $1.1 \leq m_{\mathrm{ee}} < 2.7$ GeV/$c^2$ (right), compared with the expected $\mathrm{e^+e^-}$ contributions from known hadronic decays and calculations for coherent two-photon production of dielectrons folded with the detector resolution [21, 24, 28, 36, 84]. For details see the text. The error bars and boxes represent the statistical and systematic uncertainties of the data, respectively, whereas the bands show the uncertainties of the hadronic cocktail. Arrows indicate upper limits at 90% confidence level.

The $p^2_{\mathrm{T,ee}}$ distributions of the excess $\mathrm{e^+e^-}$ pairs after subtracting the hadronic cocktail are shown in Fig. 5 for the three invariant mass regions in peripheral Pb–Pb collisions at $\sqrt{s_{\mathrm{NN}}} = 5.02$ TeV together with the different calculations for photon–photon production of dielectrons [21, 24, 28, 36, 84]. The data can be reproduced by the lowest-order QED predictions [28, 36] and computations from the authors of Ref. [21], whereas the STARlight calculation [24, 84] falls below the data points for $p^2_{\mathrm{T,ee}}$ larger than $6.25 \times 10^{-4}$ (GeV/$c$)$^2$ and overshoots the measured spectra at low $p^2_{\mathrm{T,ee}}$. This observation is consistent with the results shown as a function of $p_{\mathrm{T,ee}}$ and is in line with previous experimental measurements [22, 25, 26] which have demonstrated that the photon $k_{\mathrm{T}}$-factorization approach used in STARlight lacks $b$ dependences clearly visible in the experimental measurements. The data support the statement that the $p_{\mathrm{T,ee}}$ broadening observed in HHICs in comparison to those in UPCs originates predominantly from the initial EM field strength that varies significantly with impact parameter. To quantify the spread of the $p_{\mathrm{T,ee}}$ distributions, the $\sqrt{\langle p^2_{\mathrm{T,ee}} \rangle}$ is calculated for both the data and aforementioned photon–photon models in the measured $p^2_{\mathrm{T,ee}}$ range ($0 \leq p^2_{\mathrm{T,ee}} < 0.01$ (GeV/$c$)$^2$). The values are given in Table 2. The measured $\sqrt{\langle p^2_{\mathrm{T,ee}} \rangle}$ are found to be in agreement with expectations from theory within uncertainties. The lowest-order QED calculations and the predictions based on the Wigner formalism predict similar

$\sqrt{\langle p^2_{\mathrm{T,ee}} \rangle}$ for the three different $m_{\mathrm{ee}}$ bins. The increase observed in Table 2 is mostly due to detector $p_{\mathrm{T}}$ resolution effects. The data are not yet precise enough to conclude on a possible $m_{\mathrm{ee}}$ dependence of $\sqrt{\langle p^2_{\mathrm{T,ee}} \rangle}$.

**Table 2:** The measured $\sqrt{\langle p^2_{\mathrm{T,ee}} \rangle}$ of excess yields in 70-90% peripheral Pb–Pb collisions at $\sqrt{s_{\mathrm{NN}}}$ = 5.02 TeV compared with expectations from photon–photon calculations [21, 24, 28, 36, 84]. For details see text.

| Mass region ($\mathrm{GeV}/c^2$) | Data | QED [28, 36] | Wigner [21] | STARlight [24, 84] |
|---|---|---|---|---|
| $0.4 \leq m_{\mathrm{ee}} \leq 0.7$ | $44 \pm 28$ (stat.) $\pm 6$ (syst.) MeV/$c$ | 44 MeV/$c$ | 45 MeV/$c$ | 30 MeV/$c$ |
| $0.7 \leq m_{\mathrm{ee}} \leq 1.1$ | $45 \pm 36$ (stat.) $\pm 8$ (syst.) MeV/$c$ | 48 MeV/$c$ | 48 MeV/$c$ | 38 MeV/$c$ |
| $1.1 \leq m_{\mathrm{ee}} \leq 2.7$ | $69 \pm 36$ (stat.) $\pm 8$ (syst.) MeV/$c$ | 50 MeV/$c$ | 50 MeV/$c$ | 42 MeV/$c$ |

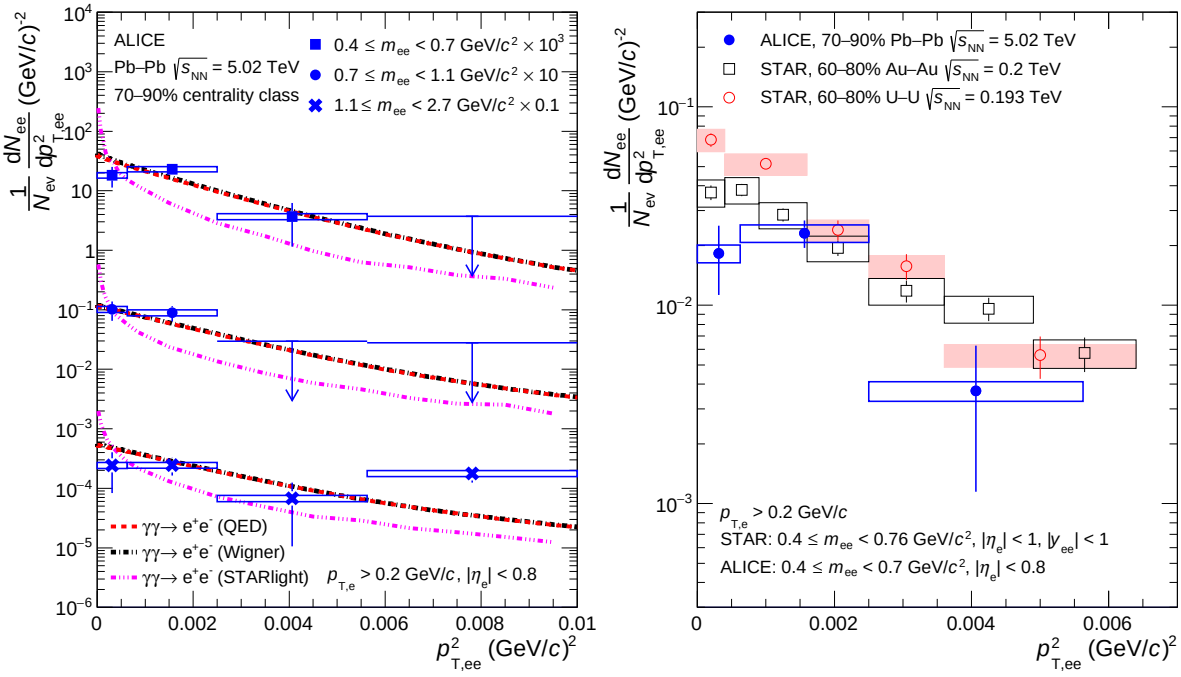


**Figure 5:** Left: Excess dielectron $p^2_{\mathrm{T,ee}}$-differential yields after subtraction of the cocktail of known hadronic decay contributions in peripheral (70–90%) Pb–Pb collisions at $\sqrt{s_{\mathrm{NN}}}$ = 5.02 TeV for different $m_{\mathrm{ee}}$ ranges, i.e. $0.4 \leq m_{\mathrm{ee}} < 0.7$ GeV/$c^2$, $0.7 \leq m_{\mathrm{ee}} < 1.1$ GeV/$c^2$ and $1.1 \leq m_{\mathrm{ee}} < 2.7$ GeV/$c^2$, compared with calculations for coherent photon–photon production of dielectrons folded with the detector resolution [21, 24, 28, 36, 84]. Right: Excess dielectron $p^2_{\mathrm{T,ee}}$-differential yields after subtraction of the cocktail of known hadronic decay contributions in peripheral Pb–Pb (70–90%), Au–Au (60–80%) and U–U (60–80%) collisions at $\sqrt{s_{\mathrm{NN}}}$ = 5.02, 0.2 and 0.193 TeV [12], respectively, in a similar $m_{\mathrm{ee}}$ range. The error bars and boxes represent the statistical and systematic uncertainties of the data, respectively. Arrows indicate upper limits at 90% confidence level.

On the right panel of Fig. 5, the measured $p^2_{\mathrm{T,ee}}$ spectrum for $0.4 \leq m_{\mathrm{ee}} < 0.7$ GeV/$c^2$ in peripheral Pb–Pb collisions is compared to the $p^2_{\mathrm{T,ee}}$ distributions measured by the STAR collaboration in a similar phase-space region in peripheral (60-80%) Au–Au and U–U collisions at $\sqrt{s_{\mathrm{NN}}}$ = 200 GeV and 193 GeV [12]. On the one hand, the $\sqrt{s_{\mathrm{NN}}}$ dependence of the cross section for the reaction $\gamma\gamma \to \mathrm{e^+e^-}$ is expected to be rather small from RHIC to LHC energies [20]. On the other hand, the $Z$ of the different colliding ions are different ($Z_{\mathrm{Au}} = 79$, $Z_{\mathrm{Pb}} = 82$, $Z_{\mathrm{U}} = 92$) and the $\eta_{\mathrm{e}}$, $y_{\mathrm{ee}}$, and $m_{\mathrm{ee}}$ ranges used in the STAR and ALICE experiments are not exactly the same. The results at LHC are found to be similar to the ones at RHIC

within large uncertainties. The measured $\sqrt{\langle p^2_{\mathrm{T,ee}} \rangle}$ (see Table 2) is comparable to the ones observed in peripheral Au–Au ($50.8 \pm 2.51$ (stat.+syst.) MeV/$c$) and U–U ($43 \pm 2.26$ (stat.+syst.) MeV/$c$) collisions.

## 5 Summary and outlook

The first measurements of $\mathrm{e^+e^-}$ pairs at low $p_{\mathrm{T,ee}}$ ($p_{\mathrm{T,ee}} < 0.1$ GeV/$c$) and $m_{\mathrm{ee}}$ ($0.4 \leq m_{\mathrm{ee}} < 2.7$ GeV/$c^2$) are presented at midrapidity ($|\eta_{\mathrm{e}}| < 0.8$) in peripheral (70–90%) and semi-peripheral (50–70%) Pb–Pb collisions at $\sqrt{s_{\mathrm{NN}}} = 5.02$ TeV. An excess of dielectrons is observed at low $p_{\mathrm{T,ee}}$ over the full measured $m_{\mathrm{ee}}$ range compared to the expected $\mathrm{e^+e^-}$ yield from known hadronic sources and thermal radiation from the medium in Pb–Pb collisions. The enhancement factors, expressed as ratios of data over hadronic cocktail, are larger in peripheral than in semi-peripheral collisions. The excess yields after subtraction of the hadronic cocktail do not exhibit a significant centrality dependence and can be reproduced as a function of $m_{\mathrm{ee}}$ by different calculations for photon–photon production of dielectrons in both centrality classes. In peripheral Pb–Pb collisions the inclusive $p_{\mathrm{T,ee}}$ spectra and the excess dielectron $p^2_{\mathrm{T,ee}}$ distributions are shown in three different $m_{\mathrm{ee}}$ intervals ($0.4 \leq m_{\mathrm{ee}} < 0.7$ GeV/$c^2$, $0.7 \leq m_{\mathrm{ee}} < 1.1$ GeV/$c^2$, and $1.1 \leq m_{\mathrm{ee}} < 2.7$ GeV/$c^2$) and compared with the hadronic cocktail and predictions for the $\gamma\gamma \to \mathrm{e^+e^-}$ process using the same models as for the $m_{\mathrm{ee}}$ spectra. The results at $p_{\mathrm{T,ee}} < 0.1$ GeV/c ($p^2_{\mathrm{T,ee}} < 0.01$ (GeV/$c$)$^2$) clearly disfavor the shape of the spectra of photon–photon produced dielectrons computed with STARlight [24, 84], whereas they are reproduced by lowest-order QED calculations [28, 36] and calculations using the Wigner formalism [21]. STARlight does not contain any impact-parameter effects on the shape of the transverse momentum distribution of the quasi-real photons and thus on the one of the $p_{\mathrm{T,ee}}$ and $p^2_{\mathrm{T,ee}}$ distributions of the produced $\mathrm{e^+e^-}$ pairs. The data show that these impact-parameter dependences cannot be neglected in non ultra-peripheral heavy-ion collisions. These results indicate that the $p_{\mathrm{T,ee}}$ broadening observed in HHICs in comparison to those in UPCs originates predominantly from the initial electromagnetic field strength that varies significantly with impact parameter. Therefore, determining precisely the magnitude of possible final-state effects related to the creation of a hot and dense medium in HHICs requires a very good understanding of the electromagnetic field produced in heavy-ion collisions. Finally, the measured $\sqrt{\langle p^2_{\mathrm{T,ee}} \rangle}$ in $0.4 \leq m_{\mathrm{ee}} < 0.7$ GeV/$c^2$ is compatible with the values observed in non-central Au–Au and U–U collisions by STAR at RHIC [12].

A significant improvement in the measurement is expected after the ALICE upgrades for the LHC Runs 3 and 4, where the number of recorded collisions for the centrality classes considered in this article is expected to increase by a factor greater than 50 [87–89]. The reduced material budget in front of the first tracking layer, as well as the improved resolution of the distance-of-closest approach to the collision vertex, will help to suppress the combinatorial and heavy-flavour backgrounds, which are particularly relevant to measure more precisely the $p_{\mathrm{T,ee}}$ distribution towards larger $p_{\mathrm{T,ee}}$ in HHIC. In addition to high precision $p_{\mathrm{T,ee}}$ or acoplanarity measurements at low $m_{\mathrm{ee}}$ in UPCs and hadronic heavy-ion Pb–Pb collisions at the LHC, more differential studies as a function of the event plane [90] and the rapidity gap between the electron and positron [32] in HHIC, as well as investigations of the $\cos(4\Delta\varphi)$ modulation as a function of $p_{\mathrm{T,ee}}$ and centrality [34], would provide further constraints on the calculations and allow possible medium effects to be investigated.

## References

[1] D. E. Kharzeev, L. D. McLerran, and H. J. Warringa, "The Effects of topological charge change in heavy ion collisions: 'Event by event P and CP violation'", *Nucl. Phys. A* **803** (2008) 227, arXiv:0711.0950 [hep-ph].

[2] M. Asakawa, A. Majumder, and B. Muller, "Electric Charge Separation in Strong Transient Magnetic Fields", *Phys. Rev. C* **81** (2010) 064912, arXiv:1003.2436 [hep-ph].

[3] K. Hattori and K. Itakura, "Vacuum birefringence in strong magnetic fields: (I) Photon polarization tensor with all the Landau levels", *Annals Phys.* **330** (2013) 23, arXiv:1209.2663 [hep-ph].

[4] V. Koch, S. Schlichting, V. Skokov, P. Sorensen, J. Thomas, S. Voloshin, G. Wang, and H.-U. Yee, "Status of the chiral magnetic effect and collisions of isobars", *Chin. Phys. C* **41** (2017) 072001, arXiv:1608.00982 [nucl-th].

[5] R. Battesti *et al.*, "High magnetic fields for fundamental physics", *Phys. Rept.* **765-766** (2018) 1, arXiv:1803.07547 [physics.ins-det].

[6] D. E. Kharzeev, J. Liao, S. A. Voloshin, and G. Wang, "Chiral magnetic and vortical effects in high-energy nuclear collisions—A status report", *Prog. Part. Nucl. Phys.* **88** (2016) 1, arXiv:1511.04050 [hep-ph].

[7] **STAR** Collaboration, B. I. Abelev *et al.*, "Azimuthal Charged-Particle Correlations and Possible Local Strong Parity Violation", *Phys. Rev. Lett.* **103** (2009) 251601, arXiv:0909.1739 [nucl-ex].

[8] **ALICE** Collaboration, B. Abelev *et al.*, "Charge separation relative to the reaction plane in Pb-Pb collisions at $\sqrt{s_{NN}} = 2.76$ TeV", *Phys. Rev. Lett.* **110** (2013) 012301, arXiv:1207.0900 [nucl-ex].

[9] **CMS** Collaboration, V. Khachatryan *et al.*, "Observation of charge-dependent azimuthal correlations in *p*-Pb collisions and its implication for the search for the chiral magnetic effect", *Phys. Rev. Lett.* **118** (2017) 122301, arXiv:1610.00263 [nucl-ex].

[10] G. Breit and J. A. Wheeler, "Collision of two light quanta", *Phys. Rev.* **46** (1934) 1087.

[11] **STAR** Collaboration, J. Adams *et al.*, "Production of $e^+e^-$ pairs accompanied by nuclear dissociation in ultra-peripheral heavy ion collision", *Phys. Rev. C* **70** (2004) 031902, arXiv:nucl-ex/0404012.

[12] **STAR** Collaboration, J. Adam *et al.*, "Low-$p_{\mathrm{T}}$ $e^+e^-$ pair production in Au+Au collisions at $\sqrt{s_{NN}}$ = 200 GeV and U+U collisions at $\sqrt{s_{NN}}$ = 193 GeV at STAR", *Phys. Rev. Lett.* **121** (2018) 132301, arXiv:1806.02295 [hep-ex].

[13] **ATLAS** Collaboration, M. Aaboud *et al.*, "Observation of centrality-dependent acoplanarity for muon pairs produced via two-photon scattering in Pb+Pb collisions at $\sqrt{s_{\mathrm{NN}}} = 5.02$ TeV with the ATLAS detector", *Phys. Rev. Lett.* **121** (2018) 212301, arXiv:1806.08708 [nucl-ex].

[14] **ATLAS** Collaboration, "Measurement of non-exclusive dimuon pairs produced via $\gamma\gamma$ scattering in Pb+Pb collisions at $\sqrt{s_{\mathrm{NN}}} = 5.02$ TeV with the ATLAS detector", *ATLAS-CONF-2019-051* (2019) .

[15] E. Fermi, "On the theory of collisions between atoms and electrically charged particles", *Nuovo Cim.* **2** (1925) 143, arXiv:hep-th/0205086.

[16] C. F. von Weizsacker, "Radiation emitted in collisions of very fast electrons", *Z. Phys.* **88** (1934) 612.

[17] E. J. Williams, "Nature of the high-energy particles of penetrating radiation and status of ionization and radiation formulae", *Phys. Rev.* **45** (1934) 729.

[18] K. Hencken, D. Trautmann, and G. Baur, "Impact parameter dependence of the total probability for the electromagnetic electron - positron pair production in relativistic heavy ion collisions", *Phys. Rev. A* **51** (1995) 1874, arXiv:nucl-th/9410014.

[19] A. Alscher, K. Hencken, D. Trautmann, and G. Baur, "Multiple electromagnetic electron positron pair production in relativistic heavy ion collisions", *Phys. Rev. A* **55** (1997) 396, arXiv:nucl-th/9606011.

[20] M. Kłusek-Gawenda, R. Rapp, W. Schäfer, and A. Szczurek, "Dilepton Radiation in Heavy-Ion Collisions at Small Transverse Momentum", *Phys. Lett. B* **790** (2019) 339, arXiv:1809.07049 [nucl-th].

[21] M. Kłusek-Gawenda, W. Schäfer, and A. Szczurek, "Centrality dependence of dilepton production via $\gamma\gamma$ processes from Wigner distributions of photons in nuclei", *Phys. Lett. B* **814** (2021) 136114, arXiv:2012.11973 [hep-ph].

[22] **ATLAS** Collaboration, G. Aad *et al.*, "Exclusive dimuon production in ultraperipheral Pb+Pb collisions at $\sqrt{s_{\mathrm{NN}}} = 5.02$ TeV with ATLAS", *Phys. Rev. C* **104** (2021) 024906, arXiv:2011.12211 [nucl-ex].

[23] **ALICE** Collaboration, E. Abbas *et al.*, "Charmonium and $\mathrm{e}^+\mathrm{e}^-$ pair photoproduction at mid-rapidity in ultra-peripheral Pb-Pb collisions at $\sqrt{s_{\mathrm{NN}}}$=2.76 TeV", *Eur. Phys. J. C* **73** (2013) 2617, arXiv:1305.1467 [nucl-ex].

[24] S. R. Klein, J. Nystrand, J. Seger, Y. Gorbunov, and J. Butterworth, "STARlight: A Monte Carlo simulation program for ultra-peripheral collisions of relativistic ions", *Comput. Phys. Commun.* **212** (2017) 258, arXiv:1607.03838 [hep-ph].

[25] **STAR** Collaboration, J. Adam *et al.*, "Measurement of $\mathrm{e}^+\mathrm{e}^-$ Momentum and Angular Distributions from Linearly Polarized Photon Collisions", *Phys. Rev. Lett.* **127** (2021) 052302, arXiv:1910.12400 [nucl-ex].

[26] **CMS** Collaboration, A. M. Sirunyan *et al.*, "Observation of Forward Neutron Multiplicity Dependence of Dimuon Acoplanarity in Ultraperipheral Pb-Pb Collisions at $\sqrt{s_{NN}}$=5.02 TeV", *Phys. Rev. Lett.* **127** (2021) 122001, arXiv:2011.05239 [hep-ex].

[27] J. D. Brandenburg, W. Li, L. Ruan, Z. Tang, Z. Xu, S. Yang, and W. Zha, "Acoplanarity of QED pairs accompanied by nuclear dissociation in ultra-peripheral heavy ion collisions", arXiv:2006.07365 [hep-ph].

[28] W. Zha, J. D. Brandenburg, Z. Tang, and Z. Xu, "Initial transverse-momentum broadening of Breit-Wheeler process in relativistic heavy-ion collisions", *Phys. Lett. B* **800** (2020) 135089, arXiv:1812.02820 [nucl-th].

[29] M. Vidovic, M. Greiner, C. Best, and G. Soff, "Impact parameter dependence of the electromagnetic particle production in ultrarelativistic heavy ion collisions", *Phys. Rev. C* **47** (1993) 2308.

[30] K. Hencken, G. Baur, and D. Trautmann, "Production of QED pairs at small impact parameter in relativistic heavy ion collisions", *Phys. Rev. C* **69** (2004) 054902, arXiv:nucl-th/0402061.

[31] C. Li, J. Zhou, and Y.-J. Zhou, "Impact parameter dependence of the azimuthal asymmetry in lepton pair production in heavy ion collisions", *Phys. Rev. D* **101** (2020) 034015, arXiv:1911.00237 [hep-ph].

[32] S. Klein, A. H. Mueller, B.-W. Xiao, and F. Yuan, "Lepton pair production through two photon process in heavy ion collisions", *Phys. Rev. D* **102** (2020) 094013, arXiv:2003.02947 [hep-ph].

[33] R.-j. Wang, S. Pu, and Q. Wang, "Lepton pair production in ultraperipheral collisions", *Phys. Rev. D* **104** (2021) 056011, arXiv:2106.05462 [hep-ph].

[34] C. Li, J. Zhou, and Y.-J. Zhou, "Probing the linear polarization of photons in ultraperipheral heavy ion collisions", *Phys. Lett. B* **795** (2019) 576, arXiv:1903.10084 [hep-ph].

[35] W. Heisenberg and H. Euler, "Consequences of Dirac's theory of positrons", *Z. Phys.* **98** (1936) 714, arXiv:physics/0605038.

[36] J. D. Brandenburg, W. Zha, and Z. Xu, "Mapping the electromagnetic fields of heavy-ion collisions with the Breit-Wheeler process", *Eur. Phys. J. A* **57** (2021) 299, arXiv:2103.16623 [hep-ph].

[37] G. Baur, "Coherent photon-photon interactions in very peripheral relativistic heavy ion collisions", *Eur. Phys. J. D* **55** (2009) 265, arXiv:0810.1400 [nucl-th].

[38] W. Zha and Z. Tang, "Discovery of higher order QED effect for the vacuum pair production", arXiv:2103.04605 [hep-ph].

[39] **ALICE** Collaboration, K. Aamodt *et al.*, "The ALICE experiment at the CERN LHC", *JINST* **3** (2008) S08002.

[40] **ALICE** Collaboration, B. B. Abelev *et al.*, "Performance of the ALICE Experiment at the CERN LHC", *Int. J. Mod. Phys. A* **29** (2014) 1430044, arXiv:1402.4476 [nucl-ex].

[41] **ALICE** Collaboration, K. Aamodt *et al.*, "Alignment of the ALICE Inner Tracking System with cosmic-ray tracks", *JINST* **5** (2010) P03003, arXiv:1001.0502 [physics.ins-det].

[42] J. Alme *et al.*, "The ALICE TPC, a large 3-dimensional tracking device with fast readout for ultra-high multiplicity events", *Nucl. Instrum. Meth. A* **622** (2010) 316, arXiv:1001.1950 [physics.ins-det].

[43] A. Akindinov *et al.*, "Performance of the ALICE Time-Of-Flight detector at the LHC", *Eur. Phys. J. Plus* **128** (2013) 44.

[44] **ALICE** Collaboration, E. Abbas *et al.*, "Performance of the ALICE VZERO system", *JINST* **8** (2013) P10016.

[45] R. Arnaldi *et al.*, "The Zero degree calorimeters for the ALICE experiment", *Nucl. Instrum. Meth. A* **581** (2007) 397. [Erratum: Nucl.Instrum.Meth.A 604, 765 (2009)].

[46] **ALICE** Collaboration, "Centrality determination in heavy ion collisions", *ALICE-PUBLIC-2018-011* (2018) . https://cds.cern.ch/record/2636623.

[47] **ALICE** Collaboration, S. Acharya *et al.*, "Dielectron production in proton-proton and proton-lead collisions at $\sqrt{s_{NN}} = 5.02$ TeV", *Phys. Rev. C* **102** (2020) 055204, arXiv:2005.11995 [nucl-ex].

[48] **ALICE** Collaboration, S. Acharya *et al.*, "Soft-dielectron excess in proton-proton collisions at $\sqrt{s}$ = 13 TeV", *Phys. Rev. Lett.* **127** (2021) 042302, arXiv:2005.14522 [nucl-ex].

[49] **ALICE** Collaboration, S. Acharya *et al.*, "Dielectron and heavy-quark production in inelastic and high-multiplicity proton–proton collisions at $\sqrt{s_{\mathrm{NN}}} = 13$TeV", *Phys. Lett. B* **788** (2019) 505, arXiv:1805.04407 [hep-ex].

[50] **PHENIX** Collaboration, A. Adare *et al.*, "Detailed measurement of the $e^+$ $e^-$ pair continuum in p+p and Au+Au collisions at $\sqrt{s_{NN}} = 200$ GeV and implications for direct photon production", *Phys. Rev. C* **81** (2010) 034911, arXiv:0912.0244 [nucl-ex].

[51] **ALICE** Collaboration, S. Acharya *et al.*, "Measurement of dielectron production in central Pb-Pb collisions at $\sqrt{s_{\mathrm{NN}}}$ = 2.76 TeV", *Phys. Rev. C* **99** (2019) 024002, arXiv:1807.00923 [nucl-ex].

[52] R. Brun, F. Bruyant, M. Maire, A. C. McPherson, and P. Zanarini, *GEANT 3: user's guide Geant 3.10, Geant 3.11; rev. version*. CERN, Geneva, 1987. https://cds.cern.ch/record/1119728.

[53] X.-N. Wang and M. Gyulassy, "HIJING: A Monte Carlo model for multiple jet production in p p, p A and A A collisions", *Phys. Rev. D* **44** (1991) 3501.

[54] P. Golonka and Z. Was, "PHOTOS Monte Carlo: A Precision tool for QED corrections in $Z$ and $W$ decays", *Eur. Phys. J. C* **45** (2006) 97, arXiv:hep-ph/0506026.

[55] T. Sjostrand, S. Mrenna, and P. Z. Skands, "PYTHIA 6.4 Physics and Manual", *JHEP* **05** (2006) 026, arXiv:hep-ph/0603175.

[56] P. Z. Skands, "Tuning Monte Carlo Generators: The Perugia Tunes", *Phys. Rev. D* **82** (2010) 074018, arXiv:1005.3457 [hep-ph].

[57] R. J. Barlow and C. Beeston, "Fitting using finite Monte Carlo samples", *Comput. Phys. Commun.* **77** (1993) 219.

[58] **ALICE** Collaboration, "Momentum transformation matrix for dielectron simulations in Pb-Pb collisions at $\sqrt{s_{\mathrm{NN}}} = 2.76$ TeV", *ALICE-PUBLIC-2017-011* (2017) . https://cds.cern.ch/record/2289779.

[59] **ALICE** Collaboration, S. Acharya *et al.*, "Dielectron production in proton-proton collisions at $\sqrt{s} = 7$ TeV", *JHEP* **09** (2018) 064, arXiv:1805.04391 [hep-ex].

[60] **WA80** Collaboration, R. Albrecht *et al.*, "Production of eta mesons in 200-A/GeV S + S and S + Au reactions", *Phys. Lett. B* **361** (1995) 14, arXiv:hep-ex/9507009.

[61] P. K. Khandai, P. Shukla, and V. Singh, "Meson spectra and $m_T$ scaling in $p+p$, $d$+Au, and Au + Au collisions at $\sqrt{s_{NN}} = 200$ GeV", *Phys. Rev. C* **84** (2011) 054904, arXiv:1110.3929 [hep-ph].

[62] L. Altenkämper, F. Bock, C. Loizides, and N. Schmidt, "Applicability of transverse mass scaling in hadronic collisions at energies available at the CERN Large Hadron Collider", *Phys. Rev. C* **96** (2017) 064907, arXiv:1710.01933 [hep-ph].

[63] **ALICE** Collaboration, S. Acharya *et al.*, "Production of charged pions, kaons, and (anti-)protons in Pb-Pb and inelastic $pp$ collisions at $\sqrt{s_{NN}}$ = 5.02 TeV", *Phys. Rev. C* **101** (2020) 044907, arXiv:1910.07678 [nucl-ex].

[64] A. A. Bylinkin and A. A. Rostovtsev, "Parametrization of the shape of hadron-production spectra in high-energy particle interactions", *Phys. Atom. Nucl.* **75** (2012) 999.

[65] A. Bylinkin, N. S. Chernyavskaya, and A. A. Rostovtsev, "Predictions on the transverse momentum spectra for charged particle production at LHC-energies from a two component model", *Eur. Phys. J. C* **75** (2015) 166, arXiv:1501.05235 [hep-ph].

[66] K. Reygers, A. Schmah, A. Berdnikova, and X. Sun, "Blast-wave description of $\Upsilon$ elliptic flow at energies available at the CERN Large Hadron Collider", *Phys. Rev. C* **101** (2020) 064905, arXiv:1910.14618 [hep-ph].

[67] G. Agakichiev *et al.*, "Neutral meson production in p−Be and p−Au collisions at 450 GeV beam energy", *Eur. Phys. J. C* **4** (1998) 249.

[68] **ALICE** Collaboration, S. Acharya *et al.*, "Production of $\omega$ mesons in pp collisions at $\sqrt{\mathbf{s}} = \mathbf{7}$ TeV", *Eur. Phys. J. C* **80** (2020) 1130, arXiv:2007.02208 [nucl-ex].

[69] **PHENIX** Collaboration, A. Adare *et al.*, "Production of $\omega$ mesons in $p+p$, d+Au, Cu+Cu, and Au+Au collisions at $\sqrt{s_N N} = 200$ GeV", *Phys. Rev. C* **84** (2011) 044902, arXiv:1105.3467 [nucl-ex].

[70] **ALICE** Collaboration, S. Acharya *et al.*, "Evidence of rescattering effect in Pb-Pb collisions at the LHC through production of $\mathrm{K}^*(892)^0$ and $\phi(1020)$ mesons", *Phys. Lett. B* **802** (2020) 135225, arXiv:1910.14419 [nucl-ex].

[71] P. Nason, "A New method for combining NLO QCD with shower Monte Carlo algorithms", *JHEP* **11** (2004) 040, arXiv:hep-ph/0409146 [hep-ph].

[72] S. Frixione, P. Nason, and G. Ridolfi, "A Positive-weight next-to-leading-order Monte Carlo for heavy flavour hadroproduction", *JHEP* **09** (2007) 126.

[73] S. Frixione, P. Nason, and C. Oleari, "Matching NLO QCD computations with Parton Shower simulations: the POWHEG method", *JHEP* **11** (2007) 070.

[74] S. Alioli, P. Nason, C. Oleari, and E. Re, "A general framework for implementing NLO calculations in shower Monte Carlo programs: the POWHEG BOX", *JHEP* **06** (2010) 043, arXiv:1002.2581 [hep-ph].

[75] G. J. Feldman and R. D. Cousins, "A Unified approach to the classical statistical analysis of small signals", *Phys. Rev. D* **57** (1998) 3873, arXiv:physics/9711021.

[76] R. Rapp and J. Wambach, "Low mass dileptons at the CERN SPS: Evidence for chiral restoration?", *Eur. Phys. J. A* **6** (1999) 415, arXiv:hep-ph/9907502.

[77] H. van Hees and R. Rapp, "Dilepton Radiation at the CERN Super Proton Synchrotron", *Nucl. Phys. A* **806** (2008) 339, arXiv:0711.3444 [hep-ph].

[78] R. Rapp, "Dilepton Spectroscopy of QCD Matter at Collider Energies", *Adv. High Energy Phys.* **2013** (2013) 148253, arXiv:1304.2309 [hep-ph].

[79] **NA60** Collaboration, R. Arnaldi *et al.*, "First measurement of the rho spectral function in high-energy nuclear collisions", *Phys. Rev. Lett.* **96** (2006) 162302, arXiv:nucl-ex/0605007.

[80] **CERES** Collaboration, D. Adamova *et al.*, "Modification of the rho-meson detected by low-mass electron-positron pairs in central Pb-Au collisions at 158-A-GeV/c", *Phys. Lett. B* **666** (2008) 425, arXiv:nucl-ex/0611022.

[81] **STAR** Collaboration, L. Adamczyk *et al.*, "Dielectron mass spectra from Au+Au Collisions at $\sqrt{s_{\mathrm{NN}}}$ = 200 GeV", *Phys. Rev. Lett.* **113** (2014) 022301, arXiv:1312.7397 [hep-ex]. [Addendum: Phys.Rev.Lett. 113, 049903 (2014)].

[82] **PHENIX** Collaboration, A. Adare *et al.*, "Dielectron production in Au+Au collisions at $\sqrt{s_{NN}}$=200 GeV", *Phys. Rev. C* **93** (2016) 014904, arXiv:1509.04667 [nucl-ex].

[83] M. Klusek-Gawenda and A. Szczurek, "Exclusive muon-pair productions in ultrarelativistic heavy-ion collisions – realistic nucleus charge form factor and differential distributions", *Phys. Rev. C* **82** (2010) 014904, arXiv:1004.5521 [nucl-th].

[84] S. R. Klein, "Two-photon production of dilepton pairs in peripheral heavy ion collisions", *Phys. Rev. C* **97** (2018) 054903, arXiv:1801.04320 [nucl-th].

[85] **ALICE** Collaboration, "Photoproduction of low-$p_{\mathrm{T}}$ J/$\psi$ from peripheral to central Pb−Pb collisions at 5.02 TeV", arXiv:2204.10684 [nucl-ex].

[86] M. B. Gay Ducati and S. Martins, "Heavy meson photoproduction in peripheral AA collisions", *Phys. Rev. D* **97** (2018) 116013, arXiv:1804.09836 [hep-ph].

[87] **ALICE** Collaboration, "Upgrade of the Inner Tracking System Conceptual Design Report. Conceptual Design Report for the Upgrade of the ALICE ITS", *CERN-LHCC-2012-013* (2012) . https://cds.cern.ch/record/1475244.

[88] **ALICE** Collaboration, "Upgrade of the ALICE Time Projection Chamber", *CERN-LHCC-2013-020* (2013) . https://cds.cern.ch/record/1622286.

[89] **ALICE** Collaboration, "Addendum to the Technical Design Report for the Upgrade of the ALICE Time Projection Chamber", *CERN-LHCC-2015-002* (2015) . https://cds.cern.ch/record/1984329.

[90] B.-W. Xiao, F. Yuan, and J. Zhou, "Momentum anisotropy of leptons from two photon processes in heavy ion collisions", *Phys. Rev. Lett.* **125** (2020) 232301, arXiv:2003.06352 [hep-ph].